Lecture 17 Form Factors

Clearly, depending on the energy and how far forward one can build a detector, would allow for the study of nuclear charge distributions via electron scattering.

What we did was in effect use $\rho(\vec{x}') = Ze\,\delta(\vec{x}')$ in

$$A^0(\vec{x}) = \int \frac{d^3\vec{x}'\,\rho(\vec{x}')}{4\pi\,|\vec{x}-\vec{x}'|}$$

In general, however, a passing electron will penetrate both the electron and nuclear electric charge distributions so,

$$\rho(\vec{x}') = n(\vec{x}') - \epsilon(\vec{x}')$$

Remember, we had $\int d^4x\, e^{-i(\pi-\vec{\pi}')\cdot\vec{x}}\, A^0(\vec{x})$ and now we consider,

$$\int d^4\vec{x} \int d^4\vec{x}' \; \frac{[n(\vec{x}') - \epsilon(\vec{x}')]\, e^{-i\vec{q}\cdot\vec{x}'}}{|\vec{x}-\vec{x}'|}$$

$$= \frac{1}{q^2} \int d\vec{x}' \,[n(\vec{x}') - \epsilon(\vec{x}')]\, e^{i\vec{q}\cdot\vec{x}'}$$

$$= \frac{1}{q^2}\,[F_N(q^2) - F_e(q^2)]$$

where I've defined the nuclear and electronic charge "Form Factors"

$$F_N(q^2) \equiv \int d^3\vec{x}\; n(\vec{x})\, e^{i\vec{q}\cdot\vec{x}}$$

$$F_e(q^2) \equiv \int d^3\vec{x}\; \epsilon(\vec{x})\, e^{i\vec{q}\cdot\vec{x}}$$

To get a feel for this thing

$$\epsilon(x) = \frac{e^{-2x/a}}{\pi a^3} \qquad a = 5\times10^{-9}\ \text{cm}, \text{ hydrogen.}$$

$$F_e(q^2) = \frac{1}{(1 + q^2a^2/4)^2}$$

if $qa >> 1$, then $F_e(q^2) \to 0$ and the electron distribution would have no effect..

$qa = 1 \Rightarrow q^2 \simeq 16\ \text{keV}^2$ pretty small

How about angle?

since $q^2 = -4E^2\sin^2\theta/2$ $\qquad \sin\theta/2 = \sqrt{q^2/4E^2}$

For very early electron beams $E \sim 100$ MeV's or so,

$\sin\theta/2 \sim 20\,\mu\text{rad} \to$ that's in the beam.

What about a more reasonable angle, like 40°?

$$-q^2 = 4(100)^2(.34)^2 \sim 5000\ \text{MeV}^2$$

$q \sim 2000$ MeV

so $qa \sim 500 \Rightarrow F_e(q^2) \sim 10^{-10} \Rightarrow$

electron cloud invisible to a modern or even old electron beam.

Had we included a finite charge distribution we would have dragged the Fourier integral through to the end

$$\frac{d\sigma}{d\Omega} = \left(\frac{d\sigma}{d\Omega}\right)_R \left(1 - \beta^2 \sin^2\theta/2\right) |F_N(q)|^2$$

$$= \left(\frac{d\sigma}{d\Omega}\right)_{point} F_N^2(q)$$

The standard interpretation of the FF is a holdover from atomic physics.

$$F(q) = \int e^{i\vec{q}\cdot\vec{r}} n(r)\, d^3r$$

$$= \int n(r)\, d^3r + \int i\vec{q}\cdot\vec{r}\, n(r)\, d^3r - \frac{1}{2}\int (\vec{q}\cdot\vec{r})^2 n(\vec{r})\, d^3r + \cdots$$

assume $n(\vec{r})$ is spherically symmetric. Since

$$\int d\Omega\, (\vec{q}\cdot\vec{r})^2 = \frac{4\pi}{3} q^2 r^2$$

$$F(q) = \int n(r)\, d^3r - \frac{1}{2}\,\frac{4\pi}{3} q^2 \int r^4 n(r)\, dr + \cdots$$

$$= \left(1 - \frac{4\pi}{6} q^2 \frac{\int r^4 n(r)\, dr}{4\pi \int r^2 n(r)\, dr} + \cdots\right) \underbrace{\int n(r)\, d^3r}_{\text{III}\ F(0)}$$

$$F(q) = \left(1 - \frac{q^2}{6}\langle r^2\rangle + \cdots\right) F(0)$$

so, one gets information on $\langle r^2 \rangle$ from a measurement of $F(q^2)$

The best fits come from exponential charge distributions — which transform into "dipole" form factors:

$$F_N(q^2) = \frac{F(0)}{\left(1 + \frac{|q^2|}{M^2}\right)^2}$$

M^2 ← a parameter of dimensions mass

The first nucleon so probed was the neutron from $n-e$ scattering in slow neutrons! From that

$$\langle r^2 \rangle \triangleq 0 \pm 0.006 \times 10^{-26} \text{ cm}^2$$

The effect of the form factor is to modulate the cross section

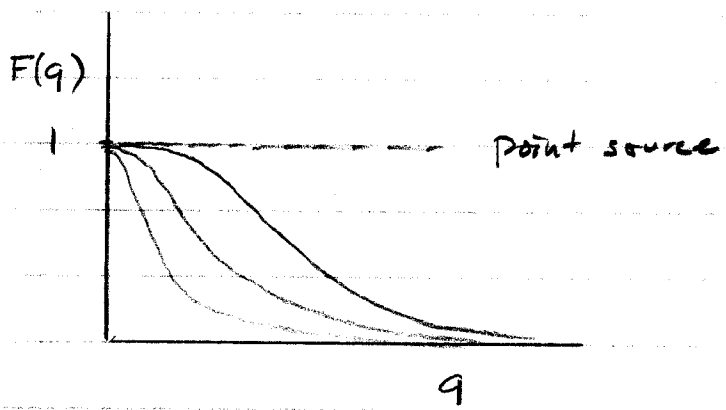

Figure 1. The effect of relativistic corrections relative to $(d\sigma/d\Omega)_R$ for 1 MeV electrons.. compared to data on Al.

Figure 2. Bottom Right.. point charge distribution predictions and Hofstadter data on 2 mil Au foil

Figure 3. Different theoretical distributions for the FF for uniform distribution (Al, Au, Ag) and shell (Au). These are relative to own $(d\sigma/d\Omega)_{point}$.

Figure 4. A part of the arsenal of distributions used as trial charge distributions by Hofstadter

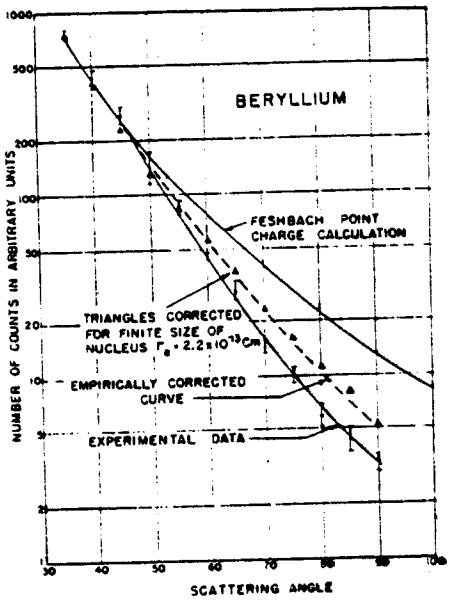

FIG. 10. The angular distribution of scattered electrons from a beryllium foil, 50-mils thick, at 125 Mev. The experimental curve has been corrected empirically for the broadening observed in the elastic curves at larger scattering angles. (See Fig. 6.) The dashed curve is the corrected curve. A theoretical curve based on the first Born approximation for an exponential charge distribution is shown. Also shown is the point charge calculation of Feshbach. Arbitrary normalization of all curves is made at 35°.

Thus, multiple scattering corrections in the target foil are unnecessary for the accuracy involved in this work. The multiple scattering in the aluminum windows is of the order of 0.4° and can be neglected since it is 4 times as small as the rms scattering angle in the gold foil. The beryllium 50-mil foil has an rms scattering angle of 0.6° which is negligible also.

The errors resulting from double (large-angle) scattering are estimated to be 0.15 percent at 90° for two mils of gold at 125 Mev and 0.01 percent at 150° under the same conditions. For 50 mils of Be at 125 Mev the errors are 1.5 percent at 150° and 0.04 percent at 90°. Hence, all double scattering corrections are ignored since they are very small effects.

The geometrical corrections for the aperture can be estimated from the effective aperture which is approximately 0.8 square inch at twelve inches. A calculation similar to that of Lyman *et al.* leads to corrections of a few tenths of a percent, which are thus negligible for our purposes.

The angular resolution of our scattering results depends on the size of the beam spot on the target foil and on the effective aperture of the entrance port of the analyzing magnet. Each of these contributions is about the same at the present time and each contributes about 2°, fairly independently of angles between 35° and 140°, for a target foil setting of 45°. Hence, our angular acceptance width is about ±4°, or a total of 8°. Structure in the scattering curves within such small angular ranges would not be resolved in our experiments. On the other hand, such fine structure is not expected.

Radiative straggling and electron-electron straggling affect the shape of the elastic-scattering peaks. Since in all the cases we have studied, with the exception of Be, the elastic profile is the same at all angles, no relative corrections for these effects need to be made. As a matter of fact, the same argument applies to the Schwinger correction.

With the exception of Be, all corrections are extremely small and will be ignored. In the case of Be (Fig. 6) the elastic profile changes as a function of angle, because of the combination of the recoil effect and the energy loss straggling in the target. Both effects are appreciable for Be. The correction has been taken into account empirically by measuring the areas under the elastic curves taken at various angles. At 90° the area is approximately 1.5 times the area at 35° when both curves are normalized to the same peak values. Hence, a correction of 50 percent is applied to the counting rate at 90°. At 35° the correction is zero, and a smooth curve has been drawn in Fig. 10 (the dashed line) to represent the corrected data at intermediate angles. Since the cross section varies rather violently with angle, the largest correction of 50 percent produces only a mild effect.

V. RESULTS

The relative angular distributions have been measured in Be, Au, and Pb at 125 Mev and in Ta at 150 Mev. In addition, as mentioned previously, check runs

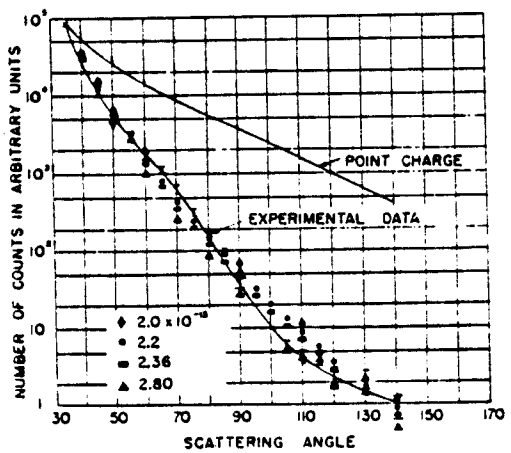

FIG. 11. The angular distribution of electrons scattered from a 2-mil gold foil at 125 Mev. The point charge calculation of Feshbach is indicated. Theoretical points based on the first Born approximation for exponential charge distributions are shown. Values of $a = 2.0$, 2.2, 2.36, 2.8×10^{-13} cm are chosen to demonstrate the sensitivity of the angular distribution to change of radius. All curves are normalized arbitrarily at 35°.

FIGURE 2

containing all nuclear particles. It does not necessarily follow that the nuclear protons are distributed over this entire volume but this is the simplest assumption.

The values for σ/σ_c as based on the work of Acheson are given in Table IV for cases of uniform and surface distributions.

V. DISCUSSION OF RESULTS

Before comparing the experimental results with the calculations of the previous section it is necessary to make the adjustment discussed previously for the effect of radiative losses associated with the observed scattering. The experimental arrangement used was not designed to check this effect accurately and hence there is only indirect experimental evidence that the correction as calculated by Schwinger and shown in Table I is correct. The agreement of the results with theory, however, is better when the radiative correction is applied. This is particularly true in the case of polystyrene and aluminum scatterers. A systematic error, such as an error in the energy of the incident beam or an error in measuring the charge incident on the foil, which could change all the observed cross sections uniformly might be wrongly interpreted in terms of a larger or smaller radiative correction. The tabulated values of δ are not expected to be accurate for high values of Z, but are used here since there are no better calculations available.

The experimental cross sections, therefore, have been adjusted for the radiative losses, δ, and are presented as ratios to the point charge scattering in Table IV. The adjusted data are shown in Fig. 4 as ratios to the simple Mott formula. This plot shows very clearly the way the scattering deviates from the simple formula. The adjusted data are presented as ratios to coulomb scattering in Fig. 5. The solid lines in this figure represent the theoretical values for a uniform nuclear charge distribution over a radius given by $1.45A^{\frac{1}{3}}\cdot 10^{-13}$ cm as used by Acheson.

Upon comparing the experimental results with the calculated values the following conclusions might be drawn. In the case of gold where the decrease in the scattering is the greatest, the results agree fairly well with the assumption that the charge is distributed uniformly over the usually accepted nuclear volume. It is apparent that the agreement would be somewhat better if a radius about 20 percent smaller than that shown in the figure is used. This indicates that the proton distribution might be more densely packed toward the center of the nucleus as suggested by Born and Yang.[26]

If it is assumed that the charge density is distributed uniformly over the surface of the nuclear volume, it is found that the observed phase shift would give a nuclear radius for gold almost a factor of two smaller than that usually accepted. Although there are reasons to expect a charge distribution which has the greatest density toward the outside of the nucleus, the present measurements seem to exclude this distribution. The decrease in the cross section for silver can also be explained in terms of a uniform distribution of charge over a 20 percent smaller radius.

It is difficult to say much about nuclear size in the cases of C, Al, and Cu since the reduction from coulomb scattering is small and of the same order of magnitude as the uncertainties in the measurements. The over-all

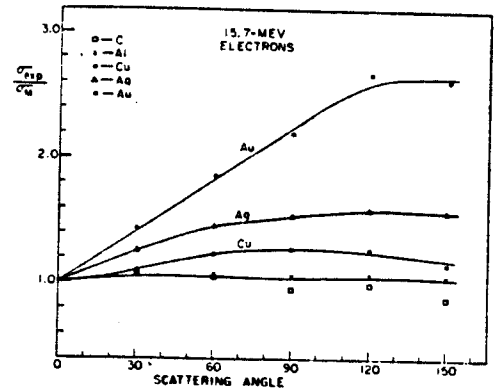

FIG. 4. Experimental results after correcting for counting losses due to radiation. The results are shown here as ratios to the simple Mott formula, Eq. (3). The solid lines sketched in are used merely to connect the experimental data and have no theoretical significance.

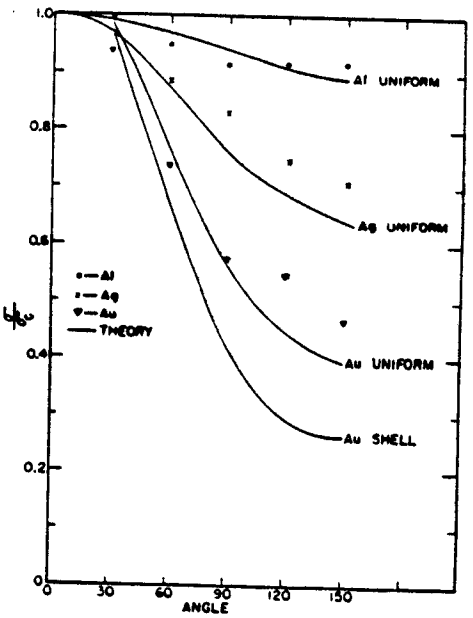

FIG. 5. Experimental results, as in Fig. 4, shown as ratios to coulomb scattering. The solid lines represent the calculated reduction in scattering for nuclear radii given by $R=1.45A^{\frac{1}{3}}\times 10^{-13}$. Calculated curves are shown only for a uniform distribution of charge except for gold where the curve for a surface charge distribution is also shown.

[26] M. Born and L. M. Yang, Nature 166, 399 (1950).

FIGURE 3

TABLE I. In this table $\rho(r)$ is the charge density function; "a" is the root-mean-square radius of the charge distribution; $F(qa)$ is the form factor; $x=qa$.

Model number	Name of model	Expression for charge density $4\pi a^3\rho(r)$; $y=r/a$	$F(qa)$; $x=qa$
I	Point	δ function	1
II	Uniform	$\frac{9}{5}\left(\frac{3}{5}\right)^{\frac{1}{2}}$ for $y\leqslant\left(\frac{5}{3}\right)^{\frac{1}{2}}$; 0 for $y\geqslant\left(\frac{5}{3}\right)^{\frac{1}{2}}$	$5\left(\frac{5}{3}\right)^{\frac{1}{2}}x^{-3}\left[\sin\left(\frac{5}{3}\right)^{\frac{1}{2}}x-\left(\frac{5}{3}\right)^{\frac{1}{2}}x\cos\left(\frac{5}{3}\right)^{\frac{1}{2}}x\right]$
III	Gaussian	$3\left(\frac{6}{\pi}\right)^{\frac{1}{2}}\exp\left(-\frac{3}{2}y^2\right)$	$\exp(-x^2/6)$
IV	Exponential	$12\sqrt{3}\exp(-(12)^{\frac{1}{2}}y)$	$\left(1+\frac{x^2}{12}\right)^{-4}$
V	Shell	$\delta(y-1)$	$x^{-1}\sin x$
VI	Hollow exponential	$\frac{200}{3}y\exp(-(20)^{\frac{1}{2}}y)$	$\left(1-\frac{x^2}{60}\right)\left(1+\frac{x^2}{20}\right)^{-4}$
VII	...	$\frac{75}{2}(30)^{\frac{1}{2}}y^2\exp(-(30)^{\frac{1}{2}}y)$	$\left(1-\frac{x^2}{30}\right)\left(1+\frac{x^2}{30}\right)^{-4}$
VIII	Yukawa I	$\sqrt{2}y^{-2}\exp(-\sqrt{2}y)$	$\sqrt{2}x^{-3}\tan^{-1}(x/\sqrt{2})$
IX	Yukawa II	$6y^{-2}\exp(-\sqrt{6}\,y)$	$\left(1+\frac{x^2}{6}\right)^{-2}$
X	Hollow Gaussian	$\frac{50}{3}\left(\frac{5}{2\pi}\right)^{\frac{1}{2}}y^2\exp\left(-\frac{5}{2}y^2\right)$	$\left(1-\frac{x^2}{15}\right)\exp\left(-\frac{x^2}{10}\right)$
XI	Generalized shell model	$\frac{8}{\sqrt{\pi}}\frac{h^3}{(2+3a)}(1+ah^2y^2)\exp(-h^2y^2)$; where $h=\left[\frac{3(2+5a)}{2(2+3a)}\right]^{\frac{1}{2}}$	$\left[1-\frac{ax^2}{2h^2(2+3a)}\right]\exp\left(-\frac{x^2}{4h^2}\right)$
XII	Modified exponential	$\frac{27}{\sqrt{2}}[1+(18)^{\frac{1}{2}}y]\exp[-(18)^{\frac{1}{2}}y]$	$\left(1+\frac{x^2}{18}\right)^{-3}$

where $\int_0^\infty 4\pi r^2\rho dr$ is normalized to unity. The ratio $r/a=y$ and is a measure of radial distance in terms of the rms radius. In Table I, x is defined as qa.

If qa is small, where a is the root-mean-square radius, all form factors reduce to the simple expansion

$$F=1-(q^2a^2/6)+\cdots. \tag{19}$$

At high energies this approximation is not useful because higher terms are needed.

Almost all useful nuclear shapes are included or approached more or less closely by one or another of the models listed in Table I. It is possible that repulsive core models are not sufficiently well approximated by any item of Table I. Several (form factors)^2 are shown in Figs. 3 and 4.

The usual procedure employed by the present author when using the Born method has been to try to fit experimental data in light nuclei with a few of the simple models. The search for a proper model is soon narrowed to one or possibly two of those given in Table I. The best fits of the parameter (or parameters) are then made.

It is also possible to invert the procedure and calculate the charge distribution from the experimental form factor. This has been done by Ravenhall[20] in analyzing accurate data on C^{12} and will be a useful procedure when the experimental data become very precise. In the author's opinion, present-day accuracy does not warrant this approach in most cases, although

[20] D. G. Ravenhall (unpublished).

FIGURE 4